Comparison of thin film and bulk forms of the transparent conducting oxide solution $Cd_{1+x}In_{2-2x}Sn_xO_4$

D. R. Kammler and T. O. Mason[a)]
Department of Materials Science and Engineering and Materials Research Center, Northwestern University, Evanston, Illinois 60208

D. L. Young and T. J. Coutts
National Renewable Energy Laboratory, Golden, Colorado 80401

D. Ko and K. R. Poeppelmeier
Department of Chemistry, Northwestern University, Evanston, Illinois 60208

D. L. Williamson
Department of Physics, Colorado School of Mines, Golden, Colorado 80401

(Received 8 June 2001; accepted for publication 13 August 2001)

Physical and structural properties of thin films prepared via rf magnetron sputtering of the transparent conducting oxide spinel $Cd_{1+x}In_{2-2x}Sn_xO_4$ are compared to those reported for bulk specimens (prepared via high-temperature solid state reaction at 1175 °C). Optical band gaps measured on thin films of $Cd_{1+x}In_{2-2x}Sn_xO_4$ were 3.5, 3.70, and 3.65 eV for $x=0.15$, 0.45, and 0.70, which where 0.57, 0.94, and 0.95 eV higher than their bulk counterparts. Thin film Seebeck coefficients were -18.0, -15.5, and -15.5 μV/K for $x=0.15$, 0.45, and 0.70, respectively, which were 27, 24, and 19 μV/K smaller in magnitude than their bulk counterparts. Sn-Mössbauer spectroscopy revealed isomer shifts that averaged 0.2 mm/s for both bulk and thin films specimens. The presence of quadrupole splitting, which averaged near 0.48 mm/s for film specimens and 0.39 mm/s for bulk specimens, suggests that Sn^{+4} in all specimens is in octahedral coordination. The difference in quadrupole splitting suggests that thin films have a different cation distribution than their bulk counterparts. The effective mass at the base of the conduction band, measured via the method-of-four-coefficients, was found to be 0.25, 0.18, 0.21, and 0.22 m_e for x equal to 0.15, 0.45, 0.70, and 1.0, respectively. A model that explains the changes in optical gap and thermopower as a result of differences in the fundamental band gap (resulting from a changing cation distribution), conduction band curvature, and carrier density is presented. © *2001 American Institute of Physics.* [DOI: 10.1063/1.1410882]

INTRODUCTION

Transparent conducting oxides (TCOs) are a class of materials that both transmit visible radiation and conduct electricity. These materials find application in numerous devices such as photovoltaics, flat-panel displays, invisible security circuits, heat reflectors, and deicers. One of the most common TCOs is indium tin oxide (ITO). Commercial grade ITO has been prepared with conductivities of 5600 S/cm, mobilities of 28.3 $cm^2/V\,s$, and carrier densities of $1.2\times10^{21}/cm^3$.[1] Given that device area is increasing, and that I^2R losses scale with device area, future TCOs need to have higher conductivities and yet maintain their transparency. Increasing conductivity by increasing the carrier density in a TCO will result in an increased absorption from free carriers. Mobility (μ) is directly proportional to the carrier relaxation time (τ) and inversely proportional to the carrier effective mass (m_c^*),[2]

$$\mu=\frac{e\tau}{m_c^*}, \tag{1}$$

where e is the electron charge. Since a decrease in the effective mass results in a shift in the free-carrier absorption band towards the visible spectrum, research efforts need to focus on increasing the relaxation time by improving existing materials or developing new ones.[3,4]

Shannon *et al.* observed that continuous edge sharing octahedra of Cd^{+2}, In^{+3}, and Sn^{+4} are a common structural feature in TCOs.[5] In addition to ITO, examples of such TCOs include the spinels, Cd_2SnO_4, and $CdIn_2O_4$. Thin films of amorphous Cd_2SnO_4 were prepared by Nozik with conductivities exceeding 1300 S/cm, mobilities of 100 $cm^2/V\,s$, and optical gaps exceeding 2.85 eV.[6] Haacke *et al.* produced thin films of polycrystalline spinel Cd_2SnO_4 with conductivities exceeding 6700 S/cm.[7] More recently, high quality films of phase pure polycrystalline Cd_2SnO_4 spinel were produced with conductivities as high as 8300 S/cm,[8] optical gaps exceeding 3.7 eV,[9] and mobilities near 77 $cm^2/V\,s$.[10] Thin films of spinel $CdIn_2O_4$ grown by Pisarkiewicz *et al.* had conductivities near 1000 S/cm and optical gaps between 2.67 and 3.24 eV.[11] Wu *et al.* produced phase pure spinel $CdIn_2O_4$ films with conductivities of 4300 S/cm and mobilities of 44 $cm^2/V\,s$.[8]

We have investigated the interior of the

a)Author to whom correspondence should be addressed; electronic mail: t-mason@northwestern.edu

$CdO-In_2O_3-SnO_2$ phase diagram in search of novel TCOs with high mobilities. Previously, we reported a bulk spinel solid solution $Cd_{1+x}In_{2-2x}Sn_xO_4$ ($0<x<0.75$ at 1175 °C) with conductivities in forming gas (96% N_2–4% H_2) annealed specimens that increased from 2200–2300 S/cm to near 3500 S/cm between $x=0.30$ and 0.6 and optical gaps that decreased from 3.0 to 2.8 eV between $x=0.1$ and 0.3.[12] Bulk Cd_2SnO_4 crystallizes in an orthorhombic form rather than in the cubic spinel form, and has poor TCO properties.[5,12] The high conductivities and wide optical gaps in $Cd_{1+x}In_{2-2x}Sn_xO_4$ prompted a thin film investigation of this solution. Thin films of this solid solution were grown by rf magnetron sputtering of targets with nominal compositions corresponding to $x=0.15$, 0.45, and 0.70. Conductivities exceeding 4000 S/cm for $x=0.45$ and 0.70, mobilities approaching 60 $cm^2/V\,s$ ($x=0.70$), carrier densities near $5.0\times10^{20}/cm^3$ ($x=0.45$ and 0.70), and optical gaps as high as 3.7 eV ($x=0.45$) were obtained.[13]

Reports that the fundamental band gaps in spinel $CdIn_2O_4$ and Cd_2SnO_4 are sensitive to the distribution of cations between tetrahedral and octahedral sites[14] prompted an investigation of the cation distribution in $Cd_{1+x}In_{2-2x}Sn_xO_4$. It was determined that the distribution evolved from primarily normal $CdIn_2O_4$ to an increasingly inverse solution as x neared the terminal point of 0.75.[15,16]

More recently, Sn-Mössbauer spectroscopy was performed on bulk and thin film polycrystalline specimens in this solution. In addition, the thermopower and density-of-states effective mass were measured in thin films in this solution using the method of four coefficients.[17] In this article we compare and contrast bulk and thin film optical band gaps, transport coefficients, and Sn-Mössbauer data. We combine these results along with the reported cation distribution[15,16] in bulk $Cd_{1+x}In_{2-2x}Sn_xO_4$ to formulate a model of the changing conduction band structure versus composition.

SPINELS: CRYSTAL STRUCTURE AND CATION DISTRIBUTIONS

Spinels are named after $MgAl_2O_4$, which has space group $Fd\bar{3}m$, cations at the special positions $8a$ (tetrahedral coordination) and $16d$ (octahedral coordination), and oxygen anions on the general positions $32e$.[18] The spinel unit cell can be constructed by combining 8 fcc unit subcells with oxygen anions at the verticies. One-half of the octahedral sites and 1/8 of the tetrahedral sites are occupied with cations. The oxygen anions can be moved along a [111] direction and thus an oxygen position parameter, u, must be specified to completely define the structure.[19] The oxygen position parameter u varies between 0.24 and 0.275 (for the setting in which the unit cell origin is at $\bar{4}3m$) and over this range the octahedral site has site symmetry $\bar{3}m$ except for $u=0.25$ where it has site symmetry $m3m$.[19] The oxygen position parameter, lattice constant, and cation radii are related through the equations below.[19]

$$R_{tet}=a\sqrt{3}(u-\tfrac{1}{8}), \tag{2}$$

$$R_{oct}=a(3u^2-2u+\tfrac{3}{8})^{1/2}. \tag{3}$$

TABLE I. Cation distribution along the ternary spinel $Cd_{1+x}In_{2-2x}Sn_xO_4$.

Cation	Tetrahedral occupancy	Octahedral occupancy	Sum
Cd^{+2}	$1-x+\lambda-\delta$	$2x-\lambda+\delta$	$1+x$
In^{+3}	δ	$2-2x-\delta$	$2-2x$
Sn^{+4}	$x-\lambda$	λ	x
Sum	1	2	3

Here R_{tet} is the tetrahedral cation-to-oxygen bond distance, R_{oct} is the octahedral cation-to-oxygen bond distance, a is the lattice constant, and u is the oxygen position parameter.

For a simple binary 2+/3+ spinel (for example, $CdIn_2O_4$), the two metal cations (Cd^{+2}, In^{+3}) can be distributed among the tetrahedral and octahedral sites according to

$$(Cd^{+2}_{1-\delta}In^{+3}_{\delta})^{tet}(Cd^{+2}_{\delta}In^{+3}_{2-\delta})^{oct}O_4 \quad (0\leqslant\delta\leqslant1), \tag{4}$$

where δ is the inversion parameter. The inversion parameter can be any value between 0 and 1. For the case when $\delta=0$ we have a ''normal'' spinel, i.e., Cd^{+2} cations on tetrahedral sites and In^{+3} cations on octahedral sites, while a value of $\delta=1$ corresponds to an ''inverse'' spinel, i.e., Cd^{+2} cations and $\frac{1}{2}$ of the In^{+3} cations on octahedral sites, with the remaining In^{+3} cations on the tetrahedral site. In a similar manner, it is possible to define an inversion parameter, λ, for the 2+/4+ spinel Cd_2SnO_4.

$$(Sn^{+4}_{1-\lambda}Cd^{+2}_{\lambda})^{tet}(Sn^{+4}_{\lambda}Cd^{+2}_{2-\lambda})^{oct}O_4 \quad (0\leqslant\lambda\leqslant1). \tag{5}$$

The possible distributions in the ternary spinel solid solution $Cd_{1+x}In_{2-2x}Sn_xO_4$ can be represented as shown below and in Table I.

$$(Cd^{+2}_{1-x+\lambda-\delta}In^{+3}_{\delta}Sn^{+4}_{x-\lambda})^{tet}(Cd^{+2}_{2x-\lambda+\delta}In^{+3}_{2-2x-\delta}Sn^{+4}_{\lambda})^{oct}O_4$$
$$(0\leqslant\delta\leqslant1-x, \quad 0\leqslant\lambda\leqslant x). \tag{6}$$

In the above case of a ternary spinel, the additional degree of freedom from the third cation make use of the words ''normal'' and ''inverse'' confusing. These words are best used for the end points (i.e., $x=0,1$) in the solution $Cd_{1+x}In_{2-2x}Sn_xO_4$. At $x=0$, δ corresponds to the inversion parameter for $CdIn_2O_4$. When $x=1$, λ corresponds to the inversion parameter for Cd_2SnO_4. The rows of Table I and the cation subscripts in Eq. (6) sum to the total Cd^{+2}, In^{+3}, and Sn^{+4} cations per formula unit for any given value of x. The columns of Table I and the subscripts within the tetrahedral and octahedral parentheses of Eq. (6) sum to 1 and 2 cations per formula unit in the tetrahedral and octahedral sites, respectively. Once the stoichiometry has been defined by fixing x, both λ and δ must be known in order to completely specify the cation distribution.

EXPERIMENTAL PROCEDURE

A complete description of the experimental procedure used to produce films of $Cd_{1+x}In_{2-2x}Sn_xO_4$ is published elsewhere.[8,9,13] Thin films of $Cd_{1+x}In_{2-2x}Sn_xO_4$ ($x=0.15$, 0.45, 0.70, and 1.0) were prepared by rf magnetron sputtering of oxide targets hot-pressed by Cerac Inc. (Milwaukee, WI) from single phase powders of identical compositions. Substrates were 2×2 in.^{2} 1.4 mm thick Corning 7059 glass

(Corning, New York). Film thickness varied between 0.1 and 1 μm. As-deposited films were subjected to a reduction anneal at temperatures between 580 and 660 °C for 20 min in atmospheres of Ar or Ar in the presence of a CdS source as described in a previous paper.[8] The CdS source was a thin film (≈800 Å) deposited on an identical substrate placed face-to-face with the as-deposited film of $Cd_{1+x}In_{2-2x}Sn_xO_4$.[20]

Both transmittance and reflectance were measured on thin films using a Cary 5 G UV/VIS/IR spectrophotometer. The thin film optical gaps were estimated from the intercept [on a plot of $(h\nu\alpha)^2$ versus $h\nu$] determined via least-squares fitting to the following equation, which assumes a direct transition between the top of the valence band and the bottom of the conduction band:[21]

$$h\nu\alpha \propto (h\nu - E_g)^{1/2}. \tag{7}$$

Here ν is the frequency of light in the transmission/reflection experiments, h is Planck's constant, E_g is the band gap, and α is the absorption coefficient, which was determined by solving Eq. (8), which is an approximation that is valid in the strongly absorbing portion of the spectrum:[9]

$$T = (1-R)^2 \exp(-\alpha t). \tag{8}$$

Here T is the transmittance, R is the reflectance, t is the film thickness, and α is the absorption coefficient.

Thin film thermopower, relaxation time, and the density-of-states effective mass were measured using the four-coefficient technique.[4,17] In this technique the Hall coefficient, thermopower, conductivity, and Nernst coefficient are measured. The latter is a proportionality constant relating the electric field developed along the *y*-direction in the presence of a thermal gradient along the *x*-direction and a magnetic field along the *z*-direction.[4] Analytical expressions for these parameters are then used to solve a system of equations arising from transport theory.[4] As a result, the carrier density, density-of-states effective mass, relaxation time, and a scattering parameter indicative of the type of scattering dominant in the film are obtained.

Mössbauer spectra were acquired in the constant acceleration mode using a 2 mCi $CaSnO_3$:^{119m}Sn source. All measurements were made with both source and absorber (the sample) at room temperature. The films on glass were mounted and electrically grounded in a conversion electron backscatter detector operated with a flow of He-10%CH_4 and an applied voltage of 950 V. Excellent signal-to-noise spectra were obtained from about 1-μm-thick films in about 48 h accumulation time per sample. The bulk specimens were fine powders mixed with fine powdered sugar and pressed into pellets of 2.5 cm diameter for transmission Mössbauer measurements. The mass of powder was adjusted depending on x to give similar excellent signal-to-noise ratios for all the bulk specimens with a 24 h accumulation time per sample. The transmission spectra were acquired with a xenon-filled proportional counter and a 50 μm Pd foil to filter the Sn x rays from the ^{119m}Snγ rays. All isomer shifts are reported relative to $CaSnO_3$. Each spectrum was least-squares-fitted with a superposition of Lorentzian line shapes. All spectra could be well-fitted (χ^2 indicator close to unity) with a quadrupole doublet with equal linewidths and intensities for the pair of lines. Alternate fits were routinely attempted that included additional single lines and quadrupole doublets but none of these resulted in improved fits compared to the single quadrupole doublet fit.

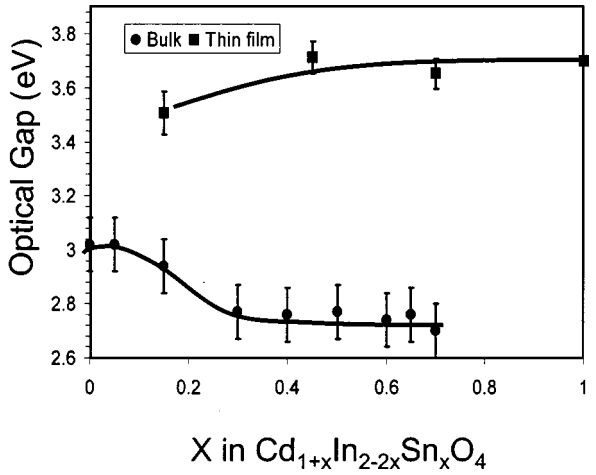

FIG. 1. Optical gaps for bulk specimens reduced in forming gas (4% H_2 and 96% N_2) and thin film specimens annealed in Ar/CdS.

RESULTS AND DISCUSSION

Figure 1 shows the optical gaps for both previously reported bulk specimens (reduced in forming gas 96% N_2:4% H_2)[12] and thin film specimens (annealed in Ar/CdS). The film specimens have substantially larger optical gaps than their bulk counterparts. Both data sets show changes in optical gap with composition. The bulk specimens show a 0.2 eV decrease in optical gap from 3.0 to 2.8 eV between $x=0.1$ and 0.3 while the thin film specimens appear to increase approximately 0.2 eV between $x=0.15$ and 0.45. A variety of factors can influence the size of the measured optical gap in a TCO, such as the fundamental band gap, a Burstein–Moss effect[22,23] effect (i.e., the upward shift in Fermi level with respect to the conduction band as states at the bottom of the conduction band are filled), and a negative contribution from band narrowing that is a consequence of an electron–electron or electron–impurity interaction.[24] Mulligan observed both Burstein–Moss and band narrowing contributions in the optical gap of spinel Cd_2SnO_4, but found the Burstein–Moss effect to dominate the shift.[9] Figure 2 shows thermopower versus composition for the previously reported bulk specimens[12] (reduced in forming gas 96% N_2:4% H_2) and the thin film specimens (annealed in Ar/CdS) in the present study. Assuming these materials are degenerate, the Fermi energy is inversely proportional to the thermopower.[25] Consequently, the bulk specimens have a substantially lower carrier density than their thin film counterparts. This suggests that the large difference in optical gap between thin film and bulk specimens is likely due to a Burstein–Moss shift. Figure 2 also shows decreasing thermopower magnitude with increasing x in both bulk and thin film specimens. This thermopower increase is consistent with an increasing carrier density as reported previously for films prepared in $Cd_{1+x}In_{2-2x}Sn_xO_4$.[13] This

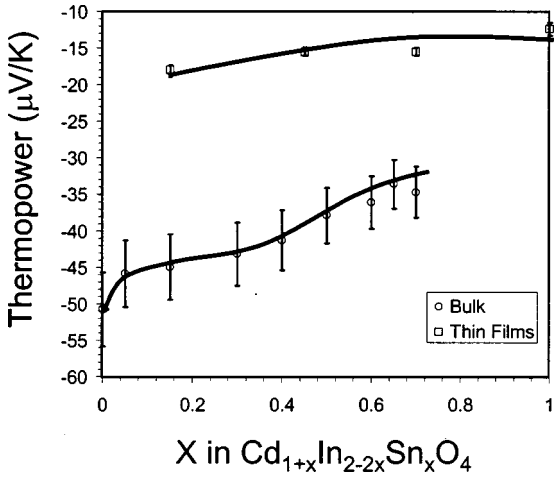

FIG. 2. Thermopower for bulk specimens reduced in forming gas (4% H_2 and 96% N_2) and thin film specimens annealed in Ar/CdS.

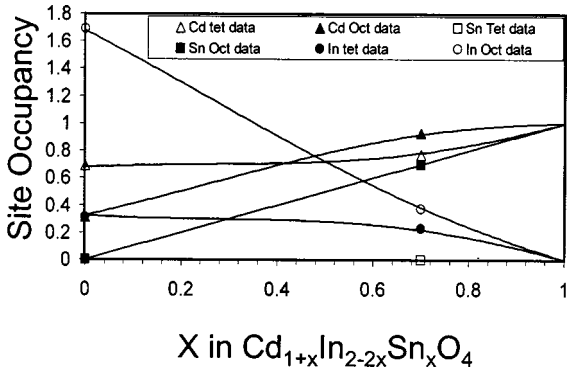

FIG. 3. Cation distribution along $Cd_{1+x}In_{2-2x}Sn_xO_4$ (after Ref. 16).

might explain the increase in optical gap with increasing x for thin film specimens but cannot explain the decrease in optical gap with x observed in bulk specimens. The fundamental band gap may be changing with x owing to changes in the cation distribution along the solution.

Wei and Zhang have shown via first principles band structure calculations that the fundamental band gaps in spinel $CdIn_2O_4$ and Cd_2SnO_4 are dependent on the inversion parameter.[14] Normal $CdIn_2O_4$ (calculated to be more stable than inverse $CdIn_2O_4$) was predicted to have a fundamental band gap 1.07 eV larger than inverse $CdIn_2O_4$, while normal Cd_2SnO_4 was calculated to have a fundamental gap 0.14 eV smaller than inverse Cd_2SnO_4 (calculated to be more stable than normal Cd_2SnO_4).[14] Clearly, knowledge of the cation distribution in the solution $Cd_{1+x}In_{2-2x}Sn_xO_4$ is important to understand the change in the fundamental band gap with composition.

Previous work using the techniques of transmission electron microscopy (TEM) atom location by channeling enhanced microanalysis (ALCHEMI), neutron diffraction, and x-ray diffraction (XRD) showed that the distribution in bulk $^{112}Cd_{1+x}In_{2-2x}Sn_xO_4$ specimens[26] (quenched from 1175 °C) evolves from primarily normal $CdIn_2O_4$ to increasingly random $^{112}Cd_{1.70}In_{0.6}Sn_{0.7}O_4$.[15,16] Using the notation in Eqs. (4)–(6) the distributions could be written as $(^{112}Cd_{0.69}In_{0.31})^{tet}(^{112}Cd_{0.31}In_{1.69})^{oct}O_4$ (i.e., $x=\lambda=0$, $\delta=0.31$) and $(^{112}Cd_{0.77}In_{0.23})^{tet}(^{112}Cd_{0.93}In_{0.37}Sn_{0.7})^{oct}O_4$ (i.e., $x=\lambda=0.70$, $\delta=0.23$).[16] Figure 3 shows a summary plot of the cation occupancies in $Cd_{1+x}In_{2-2x}Sn_xO_4$ (Ref. 16) (the smooth curves were obtained by fitting the data with the model of O'Neill and Navrotsky).[16,19,27] The different curves in Fig. 3 correspond to the different cells in Table (I) and the subscripts of each cation in Eq. (4). Figure 3 shows that up to $x\sim0.5$ the quantity of Cd^{+2} and In^{+3} on the tetrahedral sites remains essentially fixed, while $2\,In^{+3}$ cations on octahedral sites are being replaced by one Cd^{+2} and one Sn^{+4} cation. As x nears 1, there is no longer enough In^{+3} left on the octahedral site to sustain this trend. Tetrahedral In^{+3} is replaced with Cd^{+2} and octahedral In^{+3} is replaced with Sn^{+4}. The fundamental band gap in normal $CdIn_2O_4$ has been calculated to be 0.8 eV larger than that in inverse Cd_2SnO_4.[28] Based on this calculation and our experimental determination of the distribution in $Cd_{1+x}In_{2-2x}Sn_xO_4$, it appears that the fundamental band gap should decrease with increasing x.

Figure 4 shows a summary plot of the Sn-Mössbauer data for both bulk (quenched from 1175 °C) and thin film specimens (the $x=1$ data are from a previous study[9]). Both bulk and thin film specimens show nearly identical chemical or isomer shifts near 0.2 mm/s, which is consistent with earlier measurements of the isomer shift in thin films of spinel Cd_2SnO_4.[29,30] Although they differ in magnitude, both bulk and thin film specimens show measurable quadrupole splitting. Quadrupole splitting is a consequence of the interaction of the electric field gradient at the Sn^{+4} site with the nuclear quadrupole moment in ^{119}Sn.[31] Given that the tetrahedral sites in spinels have cubic symmetry and consequently no electric field gradient,[29] it would appear that the Sn^{+4} is located solely on the octahedral site in both bulk and thin film specimens. Attempts to use only single lines (corresponding to cubic Sn^{+4} sites), or add single lines to the quadrupole doublet fits, always resulted in poorer fits as indicated by the χ^2 indicator. This result is in agreement with our previous TEM and neutron diffraction results.[15,16] The fact that the thin film quadrupole splitting is slightly larger than the bulk

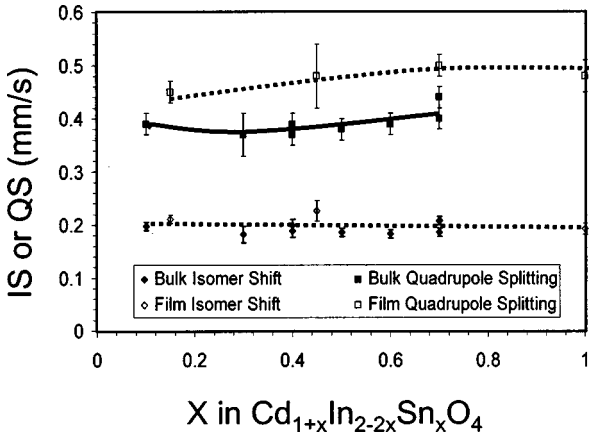

FIG. 4. Isomer shift (IS) and quadrupole splitting (QS) for bulk as-fired specimens and thin films annealed in Ar/CdS determined from Sn-Mössbauer spectroscopy data. Isomer shifts are given relative to $CaSnO_3$ ($x=1$ data after Ref. 9).

TABLE II. Calculated oxygen position parameters based on the radii of Shannon.[a]

Distribution	$CdIn_2O_4$	Cd_2SnO_4
Normal	0.262	0.246
Inverse	0.252	0.261

[a]See Ref. 32.

values suggests that the local environment around the Sn-cation is different in bulk and thin film specimens.

We have measured an oxygen position parameter between 0.262 and 0.263 for $x=0$ and 0.70 via combined x-ray and neutron diffraction refinement of data collected from bulk specimens quenched from 1175 °C.[16] While no data for u exists in films of this solution (there is insufficient material in a thin film for a neutron diffraction experiment) it is possible to speculate from the Sn-Mössbauer data how they might differ from their bulk counterparts. Given that the magnitude of the quadrupole splitting is proportional to the electric field gradient at the Sn-site,[31] the larger quadrupole splitting (shown in Fig. 4) observed in the film specimens suggests that the octahedral sites in thin films may be more distorted (i.e., further deviation from cubic symmetry caused by oxygen anions moving along $\langle 111\rangle$) and have a larger oxygen position parameter than their bulk counterparts. Table II shows calculated oxygen position parameters using Eqs. (2) and (3) and the ionic radii of Shannon.[32] For small x (i.e., close to $CdIn_2O_4$) a larger u corresponds to a more normal distribution (i.e., $x=\lambda\sim 0$, $\delta\sim 0$) while for larger x (i.e., close to Cd_2SnO_4) a larger u corresponds to a more inverse distribution (i.e., $x=\lambda\sim 1$, $\delta\sim 0$). Thus one might conclude that the cation distribution in thin films of $Cd_{1+x}In_{2-2x}Sn_xO_4$ evolves from a more normal $CdIn_2O_4$ (i.e., $\lambda_{\text{bulk}}=\lambda_{\text{film}}$; $\delta_{\text{bulk}}>\delta_{\text{film}}$) to inverse Cd_2SnO_4 (for both bulk and thin films). Thus in the film case Cd^{+2} and Sn^{+4} substitution for In^{+3} takes place almost entirely on the octahedral sublattice (as opposed to the bulk case where substitution takes place on both tetrahedral and octahedral sites for the later half of the solution). This stands to reason, given that the equilibrium distributions in the films (the film distribution will correspond to the annealing temperature of 660 °C) should be less driven by configurational entropy than their bulk counterparts (the bulk distribution will correspond to the quench temperature of 1175 °C). Consequently, the change in fundamental band gap with x in $Cd_{1+x}In_{2-2x}Sn_xO_4$ should be more extreme in films than in bulk specimens.

Figure 5 shows the density-of-states effective mass (m_d^*) measured using the method-of-four-coefficients for films of composition corresponding to $x=0.15$, 0.45, 0.70, and 1.0 in $Cd_{1+x}In_{2-2x}Sn_xO_4$. The different compositions all appear to show a gradual change in m_d^* with carrier density which indicates that the bands are not entirely parabolic. Young[4] has used a first order nonparabolic approximation to model conduction bands in TCOs that are ellipsoidal (and not parabolic) in shape and found that this model can be used to show that $(m_d^*)^2$ varies with $n^{2/3}$, with an intercept of $(m_{do}^*)^2$:

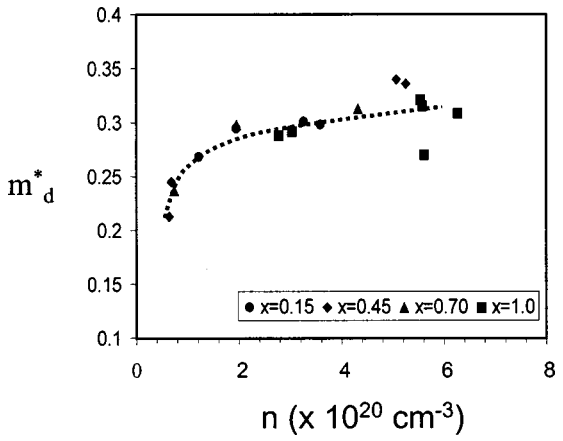

FIG. 5. Effective mass vs carrier density for thin films with compositions corresponding to $x=0.15$, 0.45, 0.70, and 1.0 along $Cd_{1+x}In_{2-2x}Sn_xO_4$.

$$(m_d^*)^2=(m_{do}^*)^2+4\frac{m_{do}^*}{E_1}\left[\left(\frac{3}{8\pi}\right)^{2/3}\frac{h^2}{2}\right]n^{2/3}. \tag{9}$$

Here m_d^* is the density-of-states effective mass, m_{do}^* is the density-of-states effective mass at the base of the conduction band, h is Plank's constant, and E_1 is a constant. This equation was used to find the effective mass at the base of the conduction band for each composition ($x=0.15$, 0.45, 0.70, and 1.0). The results of these calculations are shown in Fig. 6.

Figure 6 suggests that the curvature at the base of the conduction band shows a slight change with composition in $Cd_{1+x}In_{2-2x}Sn_xO_4$. It appears that the bands are slightly broader for $x=0.15$ and narrow as x increases to 0.45. The bands may broaden somewhat again as x approaches 1, however, the size of the error bars makes this conclusion somewhat speculative. The low effective mass at $x=0.45$ might seem to suggest that this composition could yield high mobilities, however, Fig. 5 shows that the effective mass is near $0.3m_e$ once sufficient carriers are present to produce reasonable conductivities. Furthermore, the relaxation time (τ) was found to depend on the carrier density, as shown in Fig. 7. The highest relaxation times correspond to the highest carrier

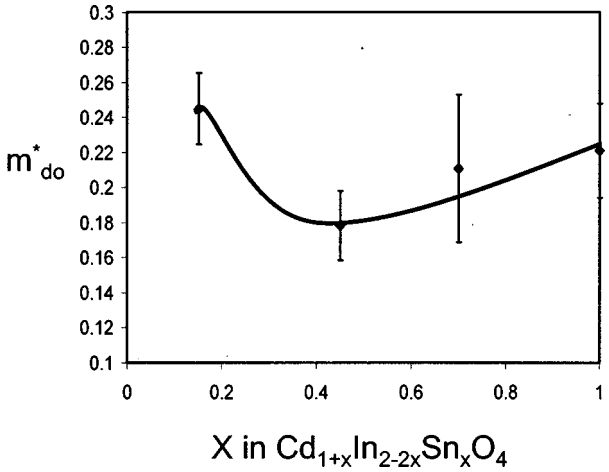

FIG. 6. Effective mass at the base of the conduction band along $Cd_{1+x}In_{2-2x}Sn_xO_4$.

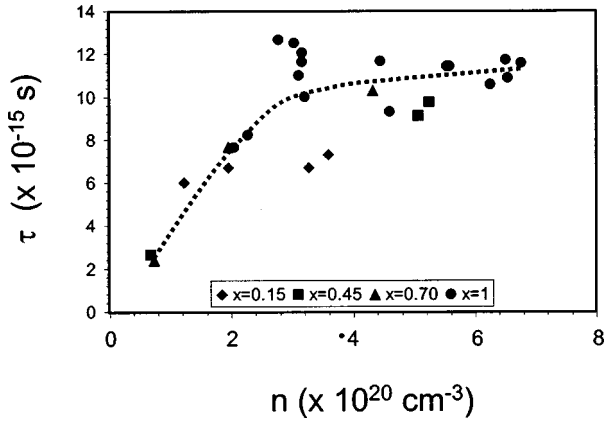

FIG. 7. Relaxation time (τ) vs carrier density (n) for $x=0.15$, 0.45, 0.70, and 1.0 along $Cd_{1+x}In_{2-2x}Sn_xO_4$.

densities, where the effective mass is the largest. Therefore there is a net cancellation of the two principal parameters (i.e., τ and m_c^*) governing mobility in Eq. (1). Relaxation time has been observed to be a strong function of carrier density in both spinel Cd_2SnO_4 and CdO TCOs as a consequence of a change in scattering mechanism.[33]

Figure 8 shows a schematic of the conduction band structure in bulk and thin film specimens that takes into account changes in fundamental band gap as a consequence of the changing cation distribution versus composition, the change in curvature of the conduction band across the solution, and the difference in carrier density between thin film and bulk specimens. The different trends in optical gap observed in Fig. 1 can now be explained. Bulk specimens show a decrease in optical gap with increasing x because the fundamental band gap associated with primarily normal $CdIn_2O_4$ is larger than that associated with inverse Cd_2SnO_4. In addition, the change in fundamental gap across the thin film solution is greater than the change in fundamental gap

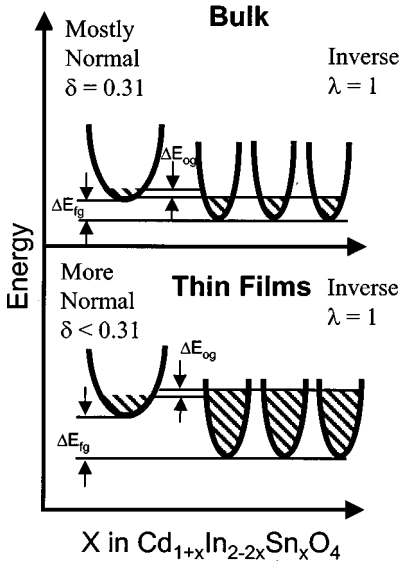

FIG. 8. Qualitative picture of the conduction bands along $Cd_{1+x}In_{2-2x}Sn_xO_4$ in bulk and thin film specimens (ΔE_{og} is the difference in optical gap, ΔE_{fg} is the difference in fundamental band gap).

across the bulk solution since the films have a cation distribution characteristic of a lower equilibrium temperature (i.e., $\delta_{bulk} > \delta_{films}$) than their bulk counterparts. As carriers fill the states at the bottom of the conduction band, the Fermi level rises and the optical gap increases as a consequence of the Burstein–Moss shift. Since the carrier density is larger near the end of the solution, the optical gaps are shifted more for larger x. Furthermore, since the curvature of the bands increases slightly with increasing x (i.e., m_{do}^* is smaller), identical carrier densities may result in increasing optical gaps with increasing x. The substantial increase in carrier density in thin films over their bulk counterparts is responsible for the increasing optical gap with increasing x observed in Fig. 1. In the bulk case, the optical gap trend is dominated by the fundamental band gap, while the thin film trend is dominated by the Burstein–Moss shift in optical gap.

CONCLUSIONS

The transport coefficients and structural properties of bulk and thin film polycrystalline specimens of the spinel transparent conducting oxide $Cd_{1+x}In_{2-2x}Sn_xO_4$ were measured. Optical gaps of 3.5, 3.70, and 3.65 eV were measured on thin films for $x=0.15$, 0.45, and 0.70, respectively. These were 0.57, 0.94, and 0.95 eV greater than their bulk counterparts. Thin film Seebeck coefficients of -18.0, -15.5, and -15.5 μV/K were measured for $x=0.15$, 0.45, and 0.70. These were 27, 24, and 19 μV/K smaller in magnitude than their bulk counterparts, which suggests that film specimens have substantially higher carrier densities than bulk specimens. Sn-Mössbauer data suggest that the octahedral site in thin films of this solution appears to be more heavily distorted than its bulk counterpart. This may indicate that the thin film cation distribution corresponds to a lower temperature equilibrium state than the bulk cation distribution in $Cd_{1+x}In_{2-2x}Sn_xO_4$. This implies that the changes in fundamental band gap with x are larger in the film specimens than their bulk counterparts. The effective mass at the base of the conduction band drops from $0.25m_e$ to $0.18m_e$ as x increases from 0 to 0.45. This change in conduction band curvature, along with changes in the size of the fundamental band gap caused by the varying cation distribution between mostly normal $CdIn_2O_4$ and inverse Cd_2SnO_4, has been used to propose a qualitative picture of changing conduction band in $Cd_{1+x}In_{2-2x}Sn_xO_4$. This model, when combined with the differing carrier densities between bulk and thin film specimens in $Cd_{1+x}In_{2-2x}Sn_xO_4$, has been used to show that the trends in optical gap in bulk specimens are dominated by the changes in fundamental gap with x in $Cd_{1+x}In_{2-2x}Sn_xO_4$, while the changes in thin film optical gaps with x are dominated by a Burstein–Moss shift.

ACKNOWLEDGMENTS

The authors are grateful to L. Brewer, S.-H. Wei, and T. Gessert for helpful discussions and to J. Keane and A. Dudda for experimental assistance. This work was supported by the U.S. Department of Energy through NREL under Subcontract No. AAD-9-18668-05 and through the MRSEC program of the National Science Foundation (Contract No.

DMR-0076097) administered through the Materials Research Center (MRC) at Northwestern University. D. R. K. received support from a National Science Foundation Graduate Fellowship.

[1] N. R. Lyman, in *Transparent Electronic Conductors* (Electrochemical Society, Hollywood, FL, 1989), pp. 201–231.
[2] T. J. Coutts, D. L. Young, and X. Li, MRS Bull. **25**, 58–65 (2000).
[3] T. J. Coutts (personal communication).
[4] D. L. Young, Doctoral thesis, Colorado School of Mines, 2000.
[5] R. D. Shannon, J. L. Gillson, and R. J. Bouchard, J. Phys. Chem. Solids **38**, 877 (1977).
[6] A. J. Nozik, Phys. Rev. B **6**, 453 (1972).
[7] G. Haacke, W. E. Mealmaker, and L. A. Siegel, Thin Solid Films **55**, 67 (1978).
[8] X. Wu, T. J. Coutts, and W. P. Mulligan, J. Vac. Sci. Technol. A **15**, 1057 (1997).
[9] W. P. Mulligan, Doctoral thesis, Colorado School of Mines, 1997.
[10] D. L. Young (personal communication).
[11] T. Pisarkiewicz, K. Zakrzewska, and E. Leja, Thin Solid Films **153**, 479 (1987).
[12] D. R. Kammler, T. O. Mason, and K. R. Poeppelmeier, Chem. Mater. **12**, 1954 (2000).
[13] D. R. Kammler, T. O. Mason, D. L. Young, and T. J. Coutts, J. Appl. Phys. **90**, 3263 (2001).
[14] S.-H. Wei and S. B. Zhang, Phys. Rev. B **63**, 45112 (2001).
[15] L. N. Brewer, D. R. Kammler, T. O. Mason, and V. P. Dravid, J. Appl. Phys. **89**, 951 (2001).
[16] D. Ko, K. R. Poeppelmeier, D. R. Kammler, and T. O. Mason, J. Solid State Chem. (to be published).
[17] D. L. Young, T. J. Coutts, and V. I. Kaydanov, Rev. Sci. Instrum. **71**, 462 (2000).
[18] R. W. G. Wyckoff, *Inorganic Compounds* $R_x(MX_4)_y$, $R_x(M_nX_p)_y$ *Hydrates and Ammoniates*, 2nd ed. (Wiley, New York, 1960), Vol. 3.
[19] H. S. C. O'Neill and A. Navrotsky, Am. Mineral. **68**, 181 (1983).
[20] This technique was developed by Dr. X. Wu at the National Renewable Energy Laboratory, Golden, CO.
[21] F. Wooten, *Optical Properties of Solids* (Academic, New York, 1972).
[22] E. Burstein, Phys. Rev. **93**, 632 (1954).
[23] T. S. Moss, Proc. Phys. Soc., London, Sect. A **382**, 775 (1954).
[24] I. Hamberg and C. G. Granqvist, J. Appl. Phys. **60**, R123 (1986).
[25] R. A. Smith, *Semiconductors*, 1st ed. (Cambridge University Press, Cambridge, England, 1961).
[26] ^{112}Cd was used because the ^{113}Cd that is present in natural Cd is a strong neutron absorber.
[27] H. S. C. O'Neill and A. Navrotsky, Am. Mineral. **69**, 733 (1984).
[28] S.-H. Wei (personal communication).
[29] T. Stapinski, E. Japa, and J. Zukrowski, Phys. Status Solidi A **103**, K93 (1987).
[30] C. M. Cardile, A. J. Koplick, R. McPherson, and B. O. West, J. Mater. Sci. Lett. **8**, 370 (1989).
[31] *Mössbauer Spectroscopy; Vol. 5*, edited by U. Gonser (Springer-Verlag, New York, 1975).
[32] R. D. Shannon, Acta Crystallogr., Sect. A: Found. Crystallogr. **A32**, 751 (1976).
[33] T. J. Coutts, D. L. Young, X. Li, W. P. Mulligan, and X. Wu, J. Vac. Sci. Technol. A **18**, 2646 (2000).